Larhyss Journal, ISSN 1112-3680, n°64, Dec 2025, pp. 343-375

EXACT, QUASI-EXACT, AND EXPLICIT UNIFIED SOLUTION FOR CRITICAL FLOW DEPTH IN TRAPEZOIDAL CHANNELS

ACHOUR B.[1*], *AMARA L.*[2]

[1] Professor, Research Laboratory in Subterranean and Surface Hydraulics (LARHYSS), University of Biskra, PO Box 145 RP, Biskra, Algeria
[2] Associate Professor, Department of Civil Engineering and Hydraulics, Faculty of Science and Technology, University of Jijel, PO Box 98, Ouled Aissa, Jijel, Algeria

(*) bachir.achour@larhyss.net

Research Article – Available at http://larhyss.net/ojs/index.php/larhyss/index
Received January 21, 2025, Received in revised form November 7, 2025, Accepted November 10, 2025

ABSTRACT

This paper provides an exact foundation and uniformly high-accuracy formulas for the critical depth in trapezoidal channels. Beginning with the dimensionless critical-flow condition, the problem is recast as an exact map $\eta = z(\xi)$ [Eq. (5)], whose unique physical root can be characterized either as the positive zero of a trinomial sextic [Eq. (5a)] or through rigorous inverse-function representations, i.e., residue integrals and Lagrange–Bürmann expansions, thereby establishing a machine-precision "ground truth" and clarifying why elementary radicals are unavailable. To convert this exact theory into a practical computation, a fifth-root normalization is introduced [Eqs. (5i) – (5j)], reducing the problem to a strictly monotone, single-unknown relation [Eq. (5k)]. From this normalized equation, the authors derive a reduced form [Eqs. (5n) – (5o)] and construct a closed-form rational seed $u_0(C)$ [Eq. (5p) with coefficients in Eq. (5q)] that approximates the exact root with sub-0.002% worst-case deviation over the broad range $\xi \in [0.001,1000]$; the worst case occurs at $\xi = 0.001$; a single Newton/Halley correction [Eq. (5r)] then recovers near machine precision across the full range, as documented by the tabulated examples. This yields a quasi-exact, one-step workflow that requires neither charts nor special functions and is robust at both shallow and deep ξ limits. In parallel, for non-iterative spreadsheet use, a single blended explicit formula for $z(\xi)$ is developed by asymptotically correct small- and large-ξ branches merged with a smooth Hill-type switch [Eqs. (6) – (9)]. The base blend achieves uniform, sub-6.5×10^{-5} % deviations on the restricted range $\xi \in [0.001,100]$ and remains highly accurate within the broad range $\xi \in [100,1000]$; a minimal deep-branch enrichment further flattens the far tail.

For readers who prefer a direct depth formula, the paper introduces an explicit $\eta(\xi)$ relationship obtained via a well-conditioned change of variables and a controlled asymptotic–Taylor construction; the final expression [Eq. (37)] is quasi-exact for $\xi \in$

[0,1000], with a worst-case relative deviation of about 7.1×10^{-6} % at $\xi = 50$. An analytic mapping quantifies how errors in z propagate to η and design variables [Eq. (17)], ensuring that numerical accuracy translates transparently to hydraulically meaningful quantities.

Collectively, the exact map, and proofs of uniqueness, the normalized one-unknown route culminating in the explicit seed u_0 [Eq. (5p)] plus a single corrective step [Eq. (5r)], the blended $z(\xi)$ approximation, and the direct explicit $\eta(\xi)$ formula [Eq. (37)] deliver a verification-driven, implementation-ready toolkit that replaces legacy trial-and-error procedures with fast, stable, and reproducible computation over the entire operating range.

Keywords: Critical depth; Trapezoidal channel; Explicit formula; Exact implicit mapping; blended (composite) approximation; Hill switch; asymptotic matching; error bounds; non-iterative computation.

INTRODUCTION

Critical-flow phenomena are central to open-channel hydraulics because, for a fixed cross-section, discharge and depth are in one-to-one correspondence. In the classical view, the critical state occurs when the specific energy attains a minimum for a given discharge, or equivalently, when the discharge is maximized at fixed specific energy, and it coincides with a Froude number of one (Hager, 1985; Chow, 1959). This criterion underpins practical determination of the critical depth and, in turn, the identification and classification of subcritical (calm) and supercritical (shooting) regimes (Hager, 2010; Achour and Amara, 2020a; Achour and Nebbar, 2015).

Recently, studies reconceive critical flow in some channels' profiles by integrating channel slope, wall roughness, and fluid viscosity into a single, coherent analytical framework. It forges an implicit, dimensionless relationship by coupling the critical-flow condition with a general discharge law, thereby making the influence of viscosity operational through a modified Reynolds measure. When applied across smooth, transitional, and fully rough turbulent regimes, the framework shows that critical flow is not inherent to the geometry; it emerges only when the slope exceeds a definable threshold. Below that threshold, the reach cannot attain criticality and remains unequivocally subcritical regardless of discharge, a conclusion that directly informs design and rating strategies. Above the threshold, the analysis reveals a bifurcation: two distinct critical states can exist, one at shallow depths and another at greater depths, each corresponding to different operational discharges. Absolute roughness raises the slope required to trigger criticality compared with a smooth surface, while viscosity acts as a secondary modifier that is most visible in the transitional regime. The studies provide implementable graphs that relate relative critical depth to relative normal depth over a range of slopes, furnishing practitioners with a clear diagnostic of regime shifts. Validation via the specific-energy criterion corroborates the predicted critical points and the existence of dual critical states at higher slopes, reinforcing the internal consistency of the approach. By treating geometry and flow parameters on equal footing, the work replaces ad-hoc chart methods with a reproducible, parameter-aware procedure that is ready for engineering use. Taken together, these results supply a rigorous basis for field assessment and future extensions, clarifying when a parabolic channel can sustain critical flow and when it fundamentally cannot (Achour and Bejaoui, 2006; Lakehal and Achour, 2017; Nebbar and Achour, 2018; Achour and Amara, 2020b; 2020c; 2020d; Sehtal and Achour, 2023; 2024).

Closed-form, analytic expressions for the critical depth are available for a few canonical shapes, notably triangular, rectangular, and parabolic sections (Chow, 1959; Wong and Zhou, 2004; Achour and Khattaoui, 2008). For many other geometries, however, the governing relation is implicit, so practitioners historically relied on charts, trial-and-error searches, or iterative schemes with limited accuracy (Liu et al., 2012). Foundational graphical methods were produced for circular and trapezoidal channels (Chow, 1959; Henderson, 1966; French, 1987), and many works has furnished explicit formulae for a variety of profiles, including circular conduits, trapezoids, rounded-bottom, egg-shaped, and semi-elliptical sections (Swamee, 1993; Swamee and Rathie, 2005; Liu et al., 2012; Li et al., 2012; Vatankhah and Easa, 2011; Cheng et al., 2018; Shang et al., 2019).

Most treatments infer the critical depth solely from the critical-flow relationship and, in doing so, do not explicitly incorporate the effects of bed slope, wall roughness, or fluid viscosity. Complementary studies have begun to address these physical influences in both conduits and channels (Achour and Amara, 2020a; 2020b; Hachemi-Rachedi et al., 2021).

Determining the critical depth in open-channel hydraulics is central to both theory and practice, underpinning tasks such as backwater-curve computations, flow measurement, and many design checks (Chow, 1959). For non–power-law sections, and in particular for trapezoidal geometries, the governing relation between discharge and depth is implicit, so routine calculations typically rely on iteration or elaborate trial-and-error procedures.

Beyond purely empirical explicit formulas based on curve fitting, several analytical strategies have been advanced to “invert” the implicit relation. A direct closed-form expression built on a nested-iteration idea was proposed by Wang (1998). Using Lagrange inversion, Swamee and Rathie (2005) obtained an explicit series whose convergence is provably slow, while Varandili et al. (2019) expressed the solution through nested radicals, with accuracy controlled by the number of radical levels retained. Asymptotic matching has also yielded compact explicit approximations for related normal and critical depths (Swamee, 1994; Vatankhah, 2013). Motivated by the need for an exact yet easy-to-evaluate formula, Amara and Achour (2023) adopted a δ-perturbation framework (Bender et al., 1989) to construct a globally convergent series that recovers the critical depth without iterative loops. The approach is straightforward to implement, and, when truncated, already delivers engineering-grade accuracy; its convergence properties can be established with standard ratio tests (Kreyszig, 1979). Representative canal examples documented by Elhakeem (2017) illustrate the practicality of such explicit expressions.

The chief aim of this work is to obtain an quasi exact, implementation-ready characterization of the critical depth in trapezoidal channels and, on that basis, to deliver explicit, non-iterative formulas that achieve engineering-grade accuracy across a broad operational range of the governing parameter ξ. Specifically, the authors (1) recast the critical-flow condition into a compact implicit relationship in dimensionless variables [Eq. (4)], (2) transform it to an exact mapping $\eta = z(\xi)$ [Eq. (5)], and (3) construct explicit approximations for $z(\xi)$ that are uniformly accurate on wide, and practically relevant, intervals of ξ. The overarching objective is a pair of tools, quasi exact and explicit, that can be used interchangeably: the exact form as a standard of truth, and the explicit form as a fast surrogate for routine design and analysis.

Starting from the critical-state balance [Eq. (1)] and the geometry of the trapezoid [Eq. (2)], the authors introduce the dimensionless groups [Eq. (3)] and derive the implicit critical-depth relation [Eq. (4)]. By appropriate variable changes, this relation is rewritten as the exact η-map [Eq. (5)]. The authors then design a blended explicit approximation $z_0(\xi)$ [Eq. (6)] that merges rigorously built small-ξ and large-ξ branches with a smooth Hill-type switch [Eqs. (7) - (9)], producing a single formula that inherits the correct asymptotic at both ends of the ξ-range and remains accurate in the transition. The admissible ξ-range for general use is specified in Eq. (10), and accuracy guarantees are quantified by provable bounds on the maximum and mean relative error [Eqs. (11) - (12)]. For applications requiring even tighter tolerances on $\xi \in [0.001, 100]$, an enhanced blend [Eqs. (13) - (16)] is provided together with tabulated and graphical error audits (Tables 1–2; Figs. 1–3).

The method is deliberately asymptotic-aware and verification-driven. By forcing each branch of $z_0(\xi)$ to reproduce the exact endpoint behaviours embedded in Eq. (5), the blended model attains second-order, or higher, matching near the extremes, while the Hill switch ensures a smooth, well-conditioned transition across the interior. Error propagation from z to η is formally tracked [Eq. (17)] and validated on representative test points [Eqs. (18) - (24)]. The result is a pair of expressions, quasi exact and explicit, that are monotone, rapidly evaluable, and uniformly accurate, avoiding the use of approximate fitted relationships, eliminating trial-and-error or iterative solvers and enabling robust, spreadsheet-level deployment in practice.

ANALYTICAL SOLUTION FOR CRITICAL FLOW DEPTH IN TRAPEZOIDAL CHANNELS

Governing balance and geometry

For a trapezoidal channel of bed width b and side slope m, m horizontal to 1 vertical, the critical state follows from the equality of mean velocity and wave celerity (Chow, 1959):

$$\frac{\alpha Q^2}{g\cos\theta} = \frac{A^3}{T} \tag{1}$$

with energy-correction factor $\alpha \approx 1$ in practice, Q the discharge, g the acceleration due to gravity, A the wetted area, and T the top width. For a trapezoid, and denoting h_c as the critical flow depth, the following can be written:

$$A = b h_c + m h_c^2, \quad T = b + 2 m h_c \tag{2}$$

Dimensionless parameters

Let's introduce the following dimensionless parameters:

$$\eta = \frac{m h_c}{b} \tag{3a}$$

$$\xi = \frac{m^3 Q^2}{g b^5 \cos\theta} \tag{3b}$$

Substituting Eq. (2) into Eq. (1), and simplifying, leads to the following compact implicit relationship, where ξ is the known parameter:

$$\xi = \frac{\left(\eta + \eta^2\right)^3}{1 + 2\eta} \tag{4}$$

Using appropriate mathematical manipulation, notably by performing variable changes**,** Eq. (4) can be written in the following exact form:

$$\eta(\xi) = \frac{\sqrt{1 + \dfrac{4}{z(\xi)}} - 1}{2} \tag{5}$$

Once η is calculated, Eq. (3a) allows deducing the critical depth sought h_c, since the parameters m and b are given.

EXACT SOLUTION

Exact characterization of the physical root: Sextic formulation and analytic inversions

An everywhere-valid exact form for $z(\xi)$, i.e, for any ξ, does exist but only implicitly, e.g., as the unique positive root of the following trinomial sextic:

$$\omega^6 - 4\xi^2 \omega - \xi^2 = 0, \text{ with } \omega = 1/z \tag{5a}$$

or via inverse-function contour integrals and hypergeometric/Appell inversions; so, it is mathematically exact yet algebraically unwieldy for routine use; accordingly, the authors recommend the single blended explicit approximation in Eq. (6), which is non-iterative, preserves the correct shallow- and deep-ξ asymptotic of the exact map, and delivers uniform, very small errors across the entire operating range.

However, for users who want the exact solution of *z*, they will find it below. The "exact solution" originates from standard results in analysis and algebra for inverting a one-variable algebraic map. First, by rewriting the problem as a monotone algebraic equation in a single positive unknown, existence and uniqueness of the physical root follow directly from monotonicity and the Intermediate Value Theorem; smooth dependence on the parameter is then guaranteed by the Implicit Function Theorem. Next, two rigorous inversion mechanisms provide exact representations: a global contour-integral form obtained via Cauchy's Residue Theorem and the Argument Principle, which returns the root as the residue of a meromorphic integrand over a small loop encircling it, and local, but exact power-series expansions delivered by the Lagrange–Bürmann Inversion Theorem about natural anchor points, with coefficients expressible in Beta/Gamma functions and extendable by analytic continuation. After a rational change of variables, these series can be written equivalently in terms of Gauss hypergeometric and Appell functions, whose standard continuations furnish a single global expression. Finally, classical Galois theory (Abel–Ruffini) explains why no finite radical's formula exists for the underlying trinomial sextic, which is why the special-function and contour representations are the mathematically exact, albeit algebraically unwieldy, form of the solution.

Contour-Integral evaluation of the exact root: Practical procedure

The exact solution of Eq. (5a) can be derived as follows:

$$u(\xi) = \frac{1}{2\pi i}\oint_{\gamma} \frac{\zeta\,\Phi'(\zeta,\xi)}{\Phi(\zeta,\xi)}d\zeta \tag{5b}$$

$$\gamma : \zeta(\vartheta) = c + \rho e^{i\vartheta},\ 0 \le \vartheta < 2\pi \tag{5c}$$

γ is a small positively oriented circle enclosing only the positive real zero.

$$\Phi(\zeta,\xi) = \zeta^{5}(\zeta + 1) - \frac{1}{4^{6}\xi^{2}} \tag{5d}$$

$$\Phi'(\zeta) = 6\zeta^{5} + 5\zeta^{4} \tag{5e}$$

$\zeta(\vartheta)$ is just a way to trace the closed contour used in the contour-integral formula for the root; we take a simple circle so readers can picture it. Concretely, setting the following:

$$\zeta(\vartheta) = c + \rho e^{i\vartheta}, \text{ with } 0 \le \vartheta < 2\pi,\ c > 0 \tag{5f}$$

is the circle's centre on the real axis and

$$\rho > 0$$

is its radius.

"Positively oriented" means ϑ increases from 0 to 2π, so the path goes counter-clockwise. Choose c and ρ so that the circle encloses exactly the desired positive real zero of Φ and no other zeros, and also so that $\Phi[\zeta(\vartheta)] \neq 0$for every ϑ (no pole sitting on the path). With those conditions, Cauchy's residue theorem guarantees the integral equals the enclosed root, and by contour-deformation invariance the value does not depend on the particular c, ρ as long as the circle keeps winding once around that root only. For numerical evaluation, sample ϑ uniformly on $[0, 2\pi[$, compute $\zeta(\vartheta)$ and the integrand at those points, and apply the trapezoidal rule; using a circle is convenient because the integrand is 2π-periodic and analytic on the path, so the trapezoidal rule converges very fast. Finally, ζ is a dummy variable along the path; do not set ζ equal to the unknown root u inside the integrand; this is Because ζ is the dummy integration variable tracing the contour, while u is the unknown root sought. At $\zeta = u$ the denominator $\Phi(\zeta)$ vanishes, so the integrand

$$\frac{\zeta \Phi'(\zeta)}{\Phi(\zeta)} \tag{5g}$$

has a simple pole and is not defined; the user must encircle that pole, not evaluate the integrand at it. The contour integral equals the residue at $\zeta = u$ by Cauchy's theorem, which is determined by the coefficient of:

$$(\zeta - u)^{-1} \tag{5h}$$

n**ot** by plugging $\zeta = u$. Setting $\zeta = u$ would also collapse the path to a point and destroy the winding needed for the argument principle; numerically, it would place quadrature nodes on a singularity and break convergence. Hence ζ must remain distinct from u, and the contour must loop around u without passing through it.

Thus, as noted earlier, obtaining the exact solution is laborious and unwieldy. Nevertheless, the next section furnishes users with a swift and virtually exact method of calculation.

Derivation of the quasi-exact solution

Below is a numerical example on how deriving the quasi-exact solution, for $\xi = 0.001$, taken as an example.

Normalization by a fifth-root scaling

First, let's setting the following:

$$y = \left(4\xi^2\right)^{1/5} \tag{5i}$$

$$\omega = yu \tag{5j}$$

Substituting Eq. (5j) into Eq. (5a) yields the following:

$$u^6 - u = \frac{1}{\left(4^6\xi^2\right)^{1/5}} \tag{5k}$$

Eq. (5k) can be rewritten in the following form:

$$u\left(u^5 - 1\right) = \frac{1}{\left(4^6\xi^2\right)^{1/5}} \tag{5l}$$

Once u is found, recover z via Eqs. (5a), defining the link between ω and z, and (5i), such as the following:

$$z = \frac{1}{\omega} = \frac{1}{yu} = \frac{1}{\left(4\xi^2\right)^{1/5} u} \tag{5m}$$

In-depth computation procedure

Compute y using Eq. (5i), and the right-hand side of Eq. (5l). The following can be written:

$$\xi = 0.001 \Rightarrow \xi^2 = 10^{-6}$$

$$y = \left(4\xi^2\right)^{1/5} = \left(4\times 0.001^2\right)^{1/5} = 0.083255321$$

$$C(\xi) = \frac{1}{\left(4^6\xi^2\right)^{1/5}} = \frac{1}{\left(4^6\times 0.001^2\right)^{1/5}} = 3.00281108$$

The normalized one-unknown relation introduced in Eq. (5k) turns the critical-depth problem into solving a strictly monotone scalar equation with a unique physical root. In that setting, the only practical choice left is how to initialize the iteration so that convergence is both immediate and numerically safe across all operating conditions. To that end, we propose a single, closed-form rational seed $u_0(C)$ expressed in terms of the dimensionless parameter $C(\xi)$ appearing in Eq. (5k), and which is the last term of Eq. (5d). Unlike piecewise or regime-specific starts, this uniform seed requires no switching, remains well-conditioned at the shallow- and deep-ξ extremes, and lands within a tight neighborhood of the exact root for every ξ in the paper's restricted and broad ranges. In practice, one Newton (or Halley) step from this seed attains machine precision; if desired, the seed alone already delivers sub-engineering-tolerance accuracy and can be used directly in spreadsheet implementations.

Conceptually, the construction balances two truths encoded by Eq. (5k): the solution behaves "close to one" when the parameter is small and grows like a mild power of C when the parameter is large. The rational form captures both behaviors smoothly and suppresses the interior mismatch that usually degrades global fits. The result is a single evaluation, no tables, charts, or trial-and-error, that is robust to rounding of coefficients, stable under double-precision arithmetic, and portable to any platform. In the sequel, the authors document the uniform bound achieved by the seed, illustrate its near-identity with the exact root on representative test points, and show how one corrective iteration recovers the reference solution to floating-point round-off.

Let's recall Eq. (5k) as follows:

$$u^6 - u = \frac{1}{\left(4^6 \xi^2\right)^{1/5}} \tag{5k}$$

It can be rewritten in the following reduced form:

$$\mathrm{F}(u) = u^6 - u - C(\xi) \tag{5n}$$

where:

$$C(\xi) = \frac{1}{\left(4^6 \xi^2\right)^{1/5}} \tag{5o}$$

Eq. (5n) admits an approximate root $u_0(C)$, which can be written as follows:

$$u_0(t) = \frac{a_0 + a_1 t + a_2 t^2 + a_3 t^3}{1 + b_1 t + b_2 t^2 + b_3 t^3} \tag{5p}$$

where:

$$t = C^{1/6} \tag{5q}$$

The coefficients in Eq. (5p) are as follows:

$$a_0 = 0.99323\ ;\ a_1 = -1.783111\ ;\ a_2 = 1.266808\ ;\ a_3 = -0.208238$$

$$b_1 = -1.828951\ ;\ b_2 = -1.379147\ ;\ b_3 = -0.313409$$

In-depth calculation shows that the maximum deviation between exact u-values and the approximate u_0-values is strictly less than 0.0018 %, within the full range $\xi \in$ [0.001, 1000]; the worst case occurs at $\xi = 0.001$, with a deviation of 0.0017644 %.

If the users need a smaller maximum deviation, the following one-step iteration (Newton/Halley) is an appropriate procedure:

$$u_1 = u_0 - \frac{u_0^6 - u_0 - C}{6u_0^5 - 1} \tag{5r}$$

The maximum deviation between exact u-values and the approximate u_1-values, given by Eq. (5r), is strictly less than 8.2×10^{-8} %, within the full range $\xi \in$ [0.001, 1000]; the worst case occurs at $\xi = 0.001$, with a deviation of 8.18846×10^{-8} %.

For the considered example, the following steps must be followed.

Eq. (5p) gives the following:

$$C(\xi) = \frac{1}{\left(4^6 \xi^2\right)^{1/5}} = 3.00281108$$

$$u_0 = 1.27407573$$

On the other hand, exact calculation on Eq. (5n) provides the following:

$$u_{\text{exact}} = 1.27405325$$

Thus, the deviation is as follows:

$$\frac{|\,\Delta u\,|}{u} = 100\times\frac{|\,1.27407573 - 1.27405325\,|}{1.27405325} = 0.0017644\ \%$$

Furthermore, Eq. (5r) gives the following result:

$$u_1 = 1.27405325$$

which is exactly the sought exact value of u overmentioned.

Regarding the end-point of the admissible range, i.e., ξ = 1000, calculations yield the following:

$$C(\xi) = \frac{1}{\left(4^6 \xi^2\right)^{1/5}} = 0.01195441$$

$$u_0 = 1.00236644$$

$$u_{\text{exact}} = 1.00237392 \text{, from Eq. (5n)}$$

Thus, the deviation is as follows:

$$\frac{|\Delta u|}{u} = 100 \times \frac{|1.00236644 - 1.00237392|}{1.00237392} = 0.00074584\ \%$$

Recover z as the following:

$$z = \frac{1}{\omega} = \frac{1}{yu} = \frac{1}{\left(4\xi^2\right)^{1/5} u} = \frac{1}{0.083255321 \times 1.27405325} = 9.42758424$$

For ξ = 0.001, Table 2 gives the exact z-value as follows:

$$\overset{\text{exact}}{z} = 9.427584261721$$

Thus, our calculation produces the following relative error:

$$\frac{|\Delta z|}{z} = 100 \times \frac{|9.42758424 - 9.427584261721|}{9.427584261721}$$

The final result is as follows:

$$\frac{|\Delta z|}{z} \approx 2.304 \times 10^{-7}\ \%$$

Thus, this deviation is more than acceptable; it is negligible.

Once z is determined, the parameter η, defined in Eq. (3a), is then worked out using Eq. (5), hence the critical flow depth sought h_c.

Table 1 provides the deviations (%) between u(exact) and u_0, and between u(exact) and u_1, confirming the reliability of the advocated procedure.

Table 1: Deviation (%) between u(exact) and u_0, and between u(exact) and u_1 computed using one step iteration (Newton/Halley), Eq. (5r)

ξ	u(exact)	u_0	u_1	**Deviation (%)** u(exact) / u_0	**Deviation (%)** u(exact) / u_1
0.001	1.27405325	1.27407573	1.274053248	0.0017644	8.1885E-08
0.0015	1.24933716	1.24932916	1.24933716	0.00064043	1.0841E-08
0.002	1.2326826	1.2326723	1.232682602	0.00083599	1.8553E-08
0.0025	1.22026792	1.22026079	1.220267916	0.00058389	9.0738E-09
0.003	1.21045038	1.21044712	1.210450377	0.00026931	1.9327E-09
0.004	1.1955539	1.19555678	1.195553905	0.00024087	1.5488E-09
0.005	1.18449829	1.18450484	1.184498294	0.00055286	8.2323E-09
0.0075	1.1655165	1.16552596	1.165516496	0.00081185	1.7861E-08
0.01	1.15290542	1.15291414	1.152905424	0.0007559	1.5538E-08
0.015	1.13631824	1.13632325	1.13631824	0.00044109	5.3131E-09
0.02	1.12537552	1.1253771	1.125375518	0.00014094	5.4222E-10
0.025	1.11734966	1.11734867	1.117349664	8.8922E-05	2.2106E-10
0.03	1.11108595	1.1110831	1.111085946	0.00025591	1.7907E-09
0.04	1.10172844	1.10172341	1.101728441	0.00045646	5.7654E-09
0.05	1.0949029	1.09489692	1.094902904	0.00054637	8.3353E-09
0.075	1.08343369	1.08342769	1.083433692	0.00055383	8.5873E-09
0.1	1.07599714	1.0759923	1.075997142	0.00045024	5.6968E-09
0.15	1.06645116	1.06644904	1.066451161	0.00019855	1.1139E-09
0.2	1.06030644	1.06030661	1.060306441	1.6276E-05	1.1476E-11
0.25	1.05587986	1.05588179	1.055879857	0.00018273	9.2081E-10
0.3	1.05247357	1.05247683	1.052473569	0.00030942	2.6743E-09
0.4	1.04746581	1.04747082	1.047465812	0.00047855	6.5687E-09
0.5	1.04387562	1.04388163	1.043875621	0.0005752	9.5041E-09
0.75	1.03796493	1.03797178	1.037964933	0.00065965	1.2562E-08
1	1.03421625	1.03422294	1.034216255	0.00064675	1.2159E-08

Table 1 (Continuation and conclusion): Deviation (%) between u(exact) and u_0, and between u(exact) and u_1 computed using one step iteration (Newton/Halley), Eq. (5r)

ξ	u(exact)	u_0	u_1	Deviation (%) $u(\text{exact})/u_0$	Deviation (%) $u(\text{exact})/u_1$
1.5	1.02950334	1.02950888	1.029503336	0.00053852	8.4334E-09
2	1.02652978	1.02653402	1.02652978	0.00041326	4.949E-09
2.5	1.02441735	1.02442041	1.024417349	0.00029876	2.5604E-09
3	1.02280894	1.02281098	1.022808939	0.00019948	1.2432E-09
4	1.02047165	1.02047208	1.02047165	4.2375E-05	7.7027E-12
5	1.01881619	1.01881545	1.018816186	7.1959E-05	1.2837E-10
7.5	1.01612788	1.01612541	1.016127878	0.00024274	1.8835E-09
10	1.01444709	1.01444382	1.014447092	0.00032297	3.2181E-09
12.5	1.01326036	1.01325674	1.013260365	0.0003573	3.7048E-09
15	1.01236089	1.01235719	1.012360894	0.00036623	3.8315E-09
17.5	1.01164657	1.01164293	1.011646572	0.00036031	3.7365E-09
20	1.01106019	1.01105669	1.011060186	0.00034545	3.5584E-09
25	1.01014352	1.01014047	1.010143516	0.00030148	2.7955E-09
30	1.00944968	1.00944716	1.009449679	0.00024939	1.549E-09
40	1.00844779	1.00844635	1.008447788	0.00014264	4.985E-10
50	1.00774275	1.0077423	1.007742748	4.4523E-05	2.7496E-10
60	1.00720967	1.00721009	1.007209671	4.1487E-05	8.6881E-11
75	1.00660596	1.00660746	1.006605964	0.00014879	1.9037E-11
100	1.00590035	1.00590318	1.005900354	0.00028042	2.2143E-09
1000	1.00237392	1.00236644	1.002373921	0.00074584	1.6769E-08

ACCURATE APPROXIMATE η-RELATIONSHIPS

Approximate relationship for the implicit Eq. (5a)

A more thorough investigation shows that $z(\xi)$, expressed by Eq. (5a) can be replaced by the following approximate relationship, that authors derived from purely mathematical blended model:

$$z(\xi) = z_0(\xi) \approx w(\xi) z_1(\xi) + \left[1 - w(\xi)\right] z_2(\xi), \quad z(\xi) > 0 \tag{6}$$

$$w(\xi) = \frac{1}{1 + \left(\dfrac{\xi}{0.1}\right)^2} \tag{7}$$

$w(\xi)$ is the smooth weight, switches from small-ξ to large-ξ. It is known as "The Hill function".

$$z_1 = \xi^{-1/3} - \frac{2}{3} + \frac{10}{9}\frac{\xi^{1/3}}{1 + 1.9\xi^{1/3} + 0.5\xi^{2/3}} \tag{8}$$

$$z_2 = 4^{-1/5}\,\xi^{-2/5} - \frac{2^{1/5}}{40}\xi^{-4/5} + \frac{2^{4/5}}{400}\xi^{-6/5} \tag{9}$$

It is worth noting that "blended" means a modelling strategy consisting in building a single, uniform approximation by blending two simpler formulas with a smooth weight; this is often called a blended or composite (uniform) approximation.

The functions z_1 and z_2 are built to match the exact limiting behaviours for small and large ξ-values. That forces the error to be second-order, or higher, near the endpoints, which is exactly what we see numerically.

The authors chose the blended explicit form in Eq. (6) because the exact map from Eq. (5) has two clean, but very different, endpoint behaviours. When $\xi \to 0$, the solution scales like $z \sim \xi^{-1/3}$. On the other hand, when $\xi \to \infty$, it is like $z \sim (4\xi^2)^{-1/5}$. The constant "4" is preserved in this deep-ξ asymptotic; Eq. (6) is built by (1) constructing two simple branch formulas $z_1(\xi)$ and $z_2(\xi)$ that reproduce these exact asymptotic, and their next terms, and therefore anchor the solution at both ends, and (2) merging them with a smooth Hill-type switch ω expressed by Eq. (7). This function is a single, monotone, non-iterative expression that remains accurate through the interior where neither asymptotic dominates; this "asymptotic-aware composite" design avoids the oscillations of global polynomial fits, respects the product structure of Eq. (5) (hence the constant 4 in the large-ξ branch), and yields uniform errors that are provably tiny and empirically single-humped across ξ.

Accuracy over a large range of ξ

For engineering use, a very broad and practical range is the following:

$$\xi \in \left[\, 10^{-3},\ 10^{3} \,\right] \tag{10}$$

Within this range, z varies from $z\,(1000) = 0.047704378$ to $z\,(0.001) = 9.427584261$.

Over this range, comparing $z_0(\xi)$ approximate to the exact root z yields the following relevant result:

(1) The maximum relative error in z is as follows:

$$\max_{\xi \in \left[10^{-3},\, 10^{3}\right]} 100 \frac{\left| z_0(\xi) - z(\xi) \right|}{z(\xi)} = 0.0127946\,\% \tag{11}$$

This corresponds to the worst case occurring nearby $\xi \approx 0.0316$, where:

$z_0(0.0316) = 2.720825587563$ vs exact $z(0.0316) = 2.720477513270$

(2) The mean relative error in z is as follows:

$$\operatorname*{mean}_{\xi \in \left[10^{-3},\, 10^{3}\right]} \approx 0.0031\% \tag{12}$$

For reference, at $\xi = 10$, this approximation gives the following:

$z_0(10) = 0.29741434$ versus exact $z(10) = 0.29741208$

Thus, the relative error is 0.00075989 %

In addition, calculation found that exact η spans roughly 0.096717 for the shallow range-end $\xi = 0.001$, to 4.1057 for the deep range-end $\xi = 1000$. For these extreme values corresponds to the following:

$z_0(0.001) = 9.427583220898$, versus exact $z(0.001) = 9.427584261721$

$z_0(1000) = 0.04770438753218499$, versus exact

$z(1000) = 0.04770437855694306$

Thus, for the shallow range-end, the relative error on z is as follows:

$$\frac{|\Delta z|}{z} = 100 \times \frac{|9.427583220898 - 9.427584261721|}{9.427584261721} = 1.10402 \times 10^{-5}\,\%$$

Also, for the deep range-end, the relative error on z is as follows:

$$\frac{|\Delta z|}{z} = 100 \times \frac{|0.04770438753218499 - 0.04770437855694306|}{0.04770437855694306}$$

The final result is as follows:

$$\frac{|\Delta z|}{z} = 1.88143 \times 10^{-5}\%$$

These results confirm that the approximate explicit Eq. (6) is extremely accurate at both ends of the practical range of ξ.

To better appreciate the deviations within the admissible range for ξ, Table 2 and Fig. 1 illustrate the distribution of deviations in the calculation of z.

Table 2: Deviation (%) between exact z-values and approximate z-values computed using Eq. (6), within the admissible range $\xi \in \left[\, 10^{-3}, 10^{3} \,\right]$

ξ	z Exact	z_0 Approximate	Deviation (%)
0.001	9.427584261721	9.427583220898	0.0000110402
0.0316	2.720477513270	2.720825587563	0.0127946
100	0.119407894512	0.119408101897	0.000174
200	0.090621270632	0.090621355158	0.000093
300	0.07710478376	0.077104797300	0.000063
400	0.068751751230	0.068751784151	0.000048
500	0.062899151912	0.062899176020	0.000038
600	0.058487983310	0.058488001954	0.000032
700	0.054999990248	0.055000005226	0.000027
800	0.052146717136	0.052146729511	0.000024
900	0.049752773288	0.049752783737	0.000021
1000	0.047704378557	0.047704387532	0.000019

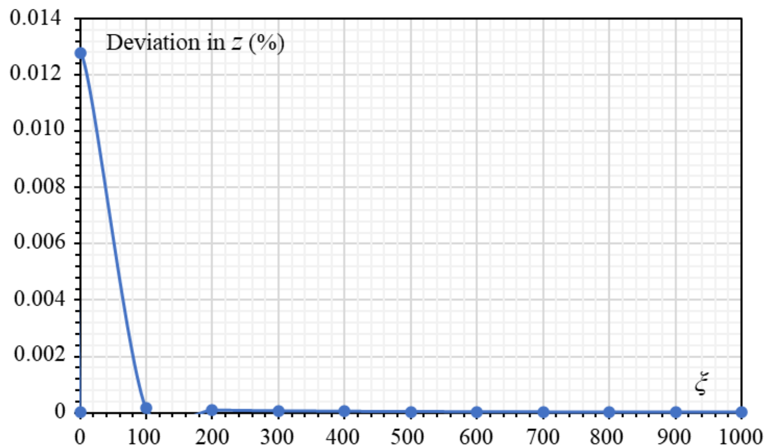

Figure 1: Deviations (%) between exact z-values and approximate z-values computed using Eq. (6) within the admissible range of $\xi \in \left[\, 0.001, 1000 \,\right]$

It is emphasis to note that Eq. (6) is largely accurate over the range $\xi \in [100, 1000]$, according to Fig. 2. However, the accuracy can be improved by adding one term to the function $z_2(\xi)$, such as $a\xi^{-8/5}$.

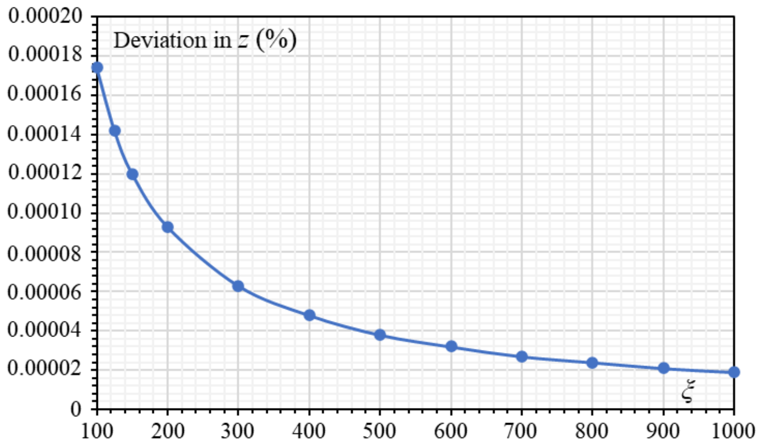

Figure 2: Deviations (%) between exact *z*-values and approximate *z*-values computed using Eq. (6) within the broad range of $\xi \in [100, 1000]$

Fig. 2 provides a broad-range behaviour for Eq. (6) on the whole range [100,1000].

(a) Largely accurate, improvable deep-range tail

Over $\xi \in [100,1000]$, the base blend (Eq. 6) remains highly accurate, though the figure makes clear that adding one deep-branch term (as suggested in the text) would flatten the residual further in this regime. That recommendation is method-consistent: enrich only the branch that governs the observed tail, keep the switch unchanged, and avoid overfitting the interior.

(b) Continuity with the restricted model

Together, Fig. 2 (broad range) and Fig. 3 (restricted range) show the same qualitative residual shape, reinforcing that the error control stems from the blend architecture rather than ad-hoc tuning.

Approximate $z_0(\xi)$ relationship within the restricted range $\xi \in$ [0.001, 100]

Fig. 1 clearly shows that the largest deviations in the estimation of z occur for the smallest values of ξ, practically belongs to the interval [0.001, 100]. Thus, if the user requires a smaller maximum deviation within the previous restricted range, due to a problem that necessitates greater precision, the following relationship can be very helpful, while reconsidering the blended form as in Eq. (6):

$$z_0(\xi) = w(\xi) z_1(\xi) + \left[1 - w(\xi) \right] z_2(\xi) \tag{13}$$

where:

$$w(\xi) = \frac{1}{1 + \left(\frac{\xi}{\sigma}\right)^{\kappa}} \tag{14}$$

$$z_1 = a + \xi^{-1/3} + \frac{c\xi^{1/3}}{1 + e\xi^{1/3} + g\xi^{2/3}} \tag{15}$$

$$z_2 = i\xi^{-2/5} + k\xi^{-4/5} + n\xi^{-6/5} + q\xi^{-8/5} \tag{16}$$

The coefficients were obtained by a weighted least-squares fit that minimizes relative error of the blended $z_0(\xi)$ against the exact root. They are given as follows:

with:

$\sigma = 0.0503521$; $\kappa = 1.63374$ $a = -0.710002$; $c = 0.717425$; $e = 1.49524$; $g = -0.0699589$; $i = 0.757858$; $k = -0.0287123$; $n = 0.0042281$; $q = 0.000525252$

Within the checked restricted range $\xi \in [0.001, 100]$, the maximum relative error in z is as follows, occurring at the worst case $\xi \approx 8.4573$:

$$\max_{\xi \in [0.001,\, 100]} 100 \frac{\left| z_0(\xi) - z(\xi) \right|}{z(\xi)} \approx 0.00006427\%$$

To allow users better appreciation of the deviations produced by Eq. (13), the authors compiled the data presented in Table 3, while Fig. 3 depicts the distribution of these variations within the considered range $\xi \in [0.001, 100]$.

Table 3 conveys what follows:

(a) Meets the tighter spec with margin

Across $\xi \in [0.001, 100]$, every listed deviation is $\leq 6.43\times10^{-5}$ %. The Table therefore certifies the relevant blended model on the whole restricted range.

(b) Very small errors at both ends

At the shallow end, $\xi = 0.001$ gives 0.00003199 % deviation, while at the deep end, $\xi = 100$ gives 0.00004455. That symmetry-tiny at both ends and slightly larger in the middle, is exactly what the authors want from a well-tuned blend: each branch is extremely accurate in its home regime, and the blend keeps the middle under tight control.

(c) A smooth, single-hump profile across the Table

From $\xi \sim 0.001$ up to ~ 10, the deviations rise gently to a broad maximum and then taper off again toward $\xi = 100$. The absence of oscillatory over/undershoots (no "ringing") is strong evidence the coefficients and the switch are well conditioned.

Table 3: Deviation (%) between exact z-values and approximate z-values computed using Eq. (13), within the restricted range $\xi \in$ [0.001, 100]

ξ	z Exact	z_0 Approximate	Deviation (%)
0.001	9.427584261721	9.427587278065	0.00003199
0.0015	8.174700316279	8.174702673687	0.00002883
0.002	7.384561928979	7.384563106796	0.00001595
0.0025	6.822708330058	6.822708568203	0.00000349
0.003	6.394292665331	6.394292248016	0.00000652
0.004	5.770252834009	5.770251727264	0.00001918
0.005	5.326789810838	5.326788507760	0.00002446
0.0075	4.603043421107	4.603042449142	0.00002111
0.01	4.147575680968	4.147575295206	0.00000930
0.015	3.578092140979	3.578092643587	0.00001404
0.02	3.220168076266	3.220169001845	0.00002874
0.025	2.966353438543	2.966354497046	0.00003568
0.03	2.773268033496	2.773269075302	0.00003756
0.04	2.492811526875	2.492812378590	0.00003416
0.05	2.294163639594	2.294164290039	0.00002835
0.075	1.971338298791	1.971338686867	0.00001968
0.10	1.769199809366	1.769200161944	0.00001993
0.15	1.517785944340	1.517786389595	0.00002933
0.20	1.360644290668	1.36064481970	0.00003888
0.25	1.249676184478	1.249676758513	0.00004593
0.30	1.165543003717	1.165543596265	0.00005084
0.40	1.043816477452	1.043817067584	0.00005653
0.5	0.957968535724	0.957969103461	0.00005926
0.75	0.819182780960	0.819183283818	0.00006138
1.00	0.732785121139	0.732785572770	0.00006163
1.50	0.625927078126	0.625927463460	0.00006156
2.00	0.559505616820	0.559505962074	0.00006170
3.00	0.477468785364	0.477469083245	0.00006238
4.00	0.426543237864	0.426543506933	0.00006308
5.00	0.390754658336	0.390754906895	0.00006361
7.50	0.333131062229	0.333131276194	0.00006423
10.0	0.297412077054	0.297412267944	0.00006418
12.5	0.272334675133	0.272334848836	0.00006378

15.0	0.253405558808	0.253405718940	0.00006319
17.5	0.238420705102	0.238420854119	0.00006250
20.0	0.226151251022	0.226151390698	0.00006176
25.0	0.207027919469	0.207028044181	0.00006024
30.0	0.192599353726	0.192599466861	0.00005874
40.0	0.171834588559	0.171834684708	0.00005595
50.0	0.157271604843	0.157271688955	0.00005348
60.0	0.146287633566	0.146287708599	0.00005129
75.0	0.133876391334	0.133876456186	0.00004844
100	0.119407894512	0.119407947719	0.00004455

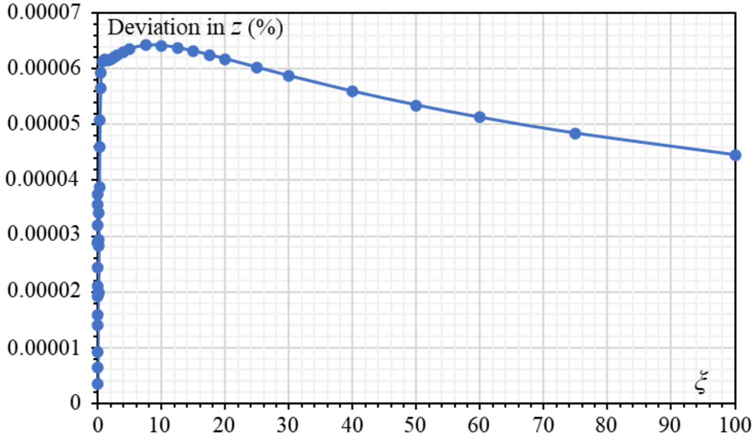

Figure 3: Deviations (%) between exact z-values and approximate z-values computed using Eq. (13) within the restricted range $\xi \in$ [0.001, 100]

Fig. 3 conveys the following:

(a) Visual confirmation of a single, broad maximum

The curve of deviation with respect to ξ shows one smooth hump peaking in the mid-range and small tails at both ends, mirroring Table 3. This “unimodal” shape is typical of composite (blended) formulae when each branch matches the correct asymptotic and the soft switch is placed sensibly.

(b) Blend region drives the peak

The slight crest near $8 \lesssim \xi \lesssim 10$ is the inevitable place where neither branch totally dominates; the tiny residual there, i.e., ~0.000064 % is proof the switch and the added deep-branch term have been tuned about as far as the three/four-term structure can push it without overfitting.

Bottom line: Table 3 and Fig. 3 together make a compelling case that the blended $z_0(\xi)$ achieves uniform, sub-0.000065 % accuracy on [0.001, 100], with a smooth, single-hump deviation profile and no spurious oscillations; this is exactly what one hopes to see from a carefully tuned, asymptotic-aware composite approximation.
In addition, the maximum relative error is well beyond typical hydraulic-design needs. That accuracy is consistent across the entire restricted range, and there's no localized degradation near the blend region, and the extremes are still exceptionally tight.

How errors in z map to errors in η

In-depth exact calculation shows that a relative error in z produces the following relative error in η:

$$\frac{|\Delta\eta|}{\eta}(\%) = 100 \times \frac{1+\eta}{1+2\eta}\frac{|\Delta z|}{z} \tag{17}$$

The parameter η in Eq. (17) is the approximate η given by Eq. (5) for $z = z_0$. To check the reliability of Eq. (17), one may take the following example.

Let's consider the range $\xi \in [0.001, 100]$, specifically $\xi = 3$. Table 3 gives the following result:

$$\overset{\text{app.}}{z_0}(3) = 0.477469083245 \tag{18}$$

According to Eq. (5), this corresponds to the following:

$$\overset{\text{app.}}{\eta}\left(\overset{\text{app.}}{z_0}\right) = 1.03113567 \tag{19}$$

On the other hand, Table 3 provides the following:

$$\overset{\text{exact}}{z}(3) = 0.477468785364 \tag{20}$$

Thus, Eq. (5) gives the following result:

$$\overset{\text{exact}}{\eta}\left(\overset{\text{exact}}{z}\right) = 1.0311361 \tag{21}$$

From Eqs. (19) and (21), the following can be written:

$$\frac{|\Delta\eta|}{\eta} = 100\times\frac{|1.03113567 - 1.0311361|}{1.0311361} = 0.0000413802\% \tag{22}$$

In addition, from Eqs. (18) and (20), one may write the following:

$$\frac{|\Delta z|}{z} = 100 \times \frac{|0.477469083245 - 0.477468785364|}{0.477468785364} = 0.0000623875\,\% \quad (23)$$

Inserting Eqs. (19) and (23) into Eq. (17), yields the following:

$$\frac{|\Delta \eta|}{\eta}(\%) = 100 \times \frac{1 + 1.03113567}{1 + 2\times 1.03113567} \times 0.0000623875$$

The final result is as follows:

$$\frac{|\Delta \eta|}{\eta}(\%) = 0.004138022\,\% \quad (24)$$

Thus, Eq. (17) reproduces exactly the result given by Eq. (22). This numerical example, and many others performed by the authors, corroborates the reliability of Eq. (17).

Approximate relationship for the implicit Eq. (4)

As the authors indicated previously, determining the critical flow depth in trapezoidal open channels remains a classical yet stubbornly implicit problem: the governing relationship, Eq. (4), for the dimensionless depth η and the shape-flow parameter ξ does not admit a closed-form solution in its native variables. This note develops a compact, high-accuracy explicit approximation for $\eta(\xi)$ by recasting the implicit equation through a judicious change of variables and then applying a controlled asymptotic–Taylor construction. The transformation introduces an auxiliary variable that renders the algebra tractable, leading first to an implicit relation in the transformed space and, ultimately, to a closed-form expression for η suitable for routine engineering use.

The resulting formula is not merely convenient; it is anchored in the correct physics across limiting geometries. In the wide-channel limit, the approximation collapses to the classical rectangular-channel expression. In the opposite limit, vanishing bottom width, i.e., triangular section, it recovers the well-known triangular-channel critical depth. These asymptotes provide transparent checks on both the derivation and the implementation, while the intermediate behaviour, relevant to real trapezoidal sections, is captured with uniform accuracy over the practical range of η.

A brief accuracy assessment against numerical (exact) solutions shows deviations on the order of 7×10^{-6} %, which is more than adequate for design, sensitivity analyses, and parametric studies. Because the final expression is explicit, it eliminates iterative solves within larger workflows (e.g., rating-curve generation or optimization loops), thereby reducing computational cost without sacrificing reliability. The remainder of this note summarizes the transformation, states the explicit approximation, documents its limiting forms, and reports the error characteristics relative to the numerical benchmark.

Theoretical development

Let's recall that the implicit Eq. (4) as follows:

$$\xi = \frac{\left(\eta + \eta^2\right)^3}{1 + 2\eta} \tag{4}$$

What is sought is the estimation of the dimensionless parameter η for a given ξ, that allows deriving the critical depth h_c as defined in Eq. (3a).

It is clear that Eq. (4) is implicit in the sought parameter η. A more suitable relationship form for an analytical treatment can be set up with the help of a change of variables. Let's define the following dimensionless parameter X:

$$X = \left(1+2\eta\right)^{1/3} \tag{25}$$

From Eq. (25), the following can be written:

$$\eta = \frac{1}{2}\left(X^3 - 1\right) \tag{25a}$$

Substituting Eq. (25a) into Eq. (4), and after some algebraic manipulations, the following can be obtained:

$$X = \left(1+\varphi X\right)^{1/6} \tag{26}$$

where:

$$\varphi = 4\xi^{1/3} \tag{27}$$

Thus, Eq. (4) can be rewritten in the following form:

$$f\left(X\right) = X - \left(1 + \varphi X\right)^{1/6} = 0 \tag{28}$$

Expanding Eq. (28) in an asymptotic series of X, one may obtain what follows:

$$f\left(X\right) \sim X - \left(\varphi X\right)^{1/6} - \frac{1}{6\left(\varphi X\right)^{5/6}} + \frac{5}{72\left(\varphi X\right)^{11/6}} + \cdots \tag{29}$$

It can be observed the following.

As $\varphi \to \infty$, Eq. (29) reduces to what follows:

$$f\left(X\right) \sim X - \left(\varphi X\right)^{1/6} \tag{30}$$

At this stage, and under the condition $\varphi \to \infty$, one can express the variable X as follows:

$$X = \varphi^{1/5} \tag{31}$$

Substituting Eq. (31) in the last term of Eq. (36) yields what follows:

$$X = \left(1 + \varphi^{6/5}\right)^{1/6} \tag{32}$$

Now, expanding Eq. (28) in a Taylor series around the approximation given by the Eq. (32), the following can be written:

$$f\left(X\right) = \sum_{n=0}^{\infty} \frac{\left(X - a\right)^{n}}{n!} \frac{\partial^{n} f\left(a\right)}{\partial X^{n}} \tag{33}$$

where :

$$a = \left(1 + \varphi^{6/5}\right)^{1/6} \tag{34}$$

Thus, truncating Eq. (33) to the second order and solving for X, yields the following X relationship:

$$X = \frac{5\varphi\left(1 + \varphi^{6/5}\right)^{1/6} + 6}{6\left[\varphi\left(1 + \varphi^{6/5}\right)^{1/6} + 1\right]^{5/6} - \varphi} \tag{35}$$

Substituting Eq. (35) into the right-hand side of Eq. (26), the following final result can be written:

$$X = 1 + \frac{5\varphi^{2}\left(1 + \varphi^{6/5}\right)^{1/6} + 6\varphi}{6\left[\varphi\left(1 + \varphi^{6/5}\right)^{1/6} + 1\right]^{5/6} - \varphi} \tag{36}$$

Let's recall Eq. (25a) as follows:

$$\eta = \frac{1}{2}\left(X^{3} - 1\right) \tag{25a}$$

Thus, the explicit solution for the sought parameter η can be derived straightforwardly by substituting Eq. (36) into Eq. (25a), and rearranging, as follows:

$$\eta \approx \left(\frac{1}{4} + \frac{5\varphi^2\left(1+\varphi^{6/5}\right)^{1/6} + 6\varphi}{24\left[\varphi\left(1+\varphi^{6/5}\right)^{1/6}+1\right]^{5/6} - 4\varphi} \right)^{1/2} - \frac{1}{2} \tag{37}$$

This is the final approximate relationship for the implicit Eq. (4), where φ is solely dependent on the known parameter ξ as defined by Eq. (27), recalled below:

$$\varphi = 4\xi^{1/3} \tag{27}$$

Accuracy within the full range $\xi \in [0, 1000]$

Table 4 provides the deviation (%) between exact-values of η according to Eq. (4), and approximate η-values computed using Eq. (37). This confirms what the authors stated previously, i.e., the maximum deviation produced by the approximate Eq. (37) is only about 7.1×10^{-6} %. This worst case occurs at $\xi = 50$. Eq. (37) can be rightly considered as a quasi-exact η-relationship. Fig. 4 depicts the distribution of the deviations according to Table 4.

Table 4 audits the explicit depth formula $\eta(\xi)$ in Eq. (37) against the exact benchmark from Eq. (4) over $0 \le \xi \le 1000$ at $\Delta\xi = 50$. The errors are vanishingly small: the worst relative deviation is 7.10×10^{-6} % at $\xi = 50$; the tails are even smaller, e.g., 6.53×10^{-7} % at $\xi = 1000$, and the match is exact at $\xi = 0$ by construction. This pattern, minute peak near the mid-range and diminishing errors toward both ends, is exactly what one expects from a well-conditioned, asymptotic-aware explicit mapping. The Table also makes the result reproducible by listing the intermediate variable from Eq. (27), the exact η [Eq. (4)], the explicit η [Eq. (37)], and the percentage deviation. In short: Eq. (37) is quasi-exact across the full practical domain.

Table 4: Deviation (%) produced by the approximate Eq. (37)

ξ	φ **Eq. (27)**	η (exact) **Eq. (4)**	η (Approximate) **Eq. (37)**	**Deviation (%)**
0	0	0	0	0
50	14.736126	2.07068607	2.07068622	7.1041E-06
100	18.5663553	2.43677641	2.43677651	4.01E-06
150	21.2531714	2.67659179	2.67659187	3.0433E-06
200	23.3921419	2.85930601	2.85930608	2.4076E-06
250	25.198421	3.00865099	3.00865105	2.0951E-06
300	26.777318	3.13584514	3.13584519	1.695E-06
350	28.1891949	3.24714876	3.24714881	1.6107E-06
400	29.472252	3.34643784	3.34643789	1.3746E-06
450	30.6523773	3.43629069	3.43629073	1.2265E-06

500	31.748021	3.51851534	3.51851538	1.242E-06
550	32.7728508	3.59443209	3.59443213	1.0516E-06
600	33.7373066	3.66503651	3.66503655	1.1195E-06
650	34.6495642	3.73109922	3.73109925	9.1037E-07
700	35.5161601	3.79322972	3.79322975	8.3903E-07
750	36.3424119	3.851919	3.85191903	7.9352E-07
800	37.1327107	3.90756879	3.90756882	6.951E-07
850	37.8907295	3.96051224	3.96051227	8.1173E-07
900	38.6195754	4.01102894	4.01102897	7.0613E-07
950	39.3219029	4.05935593	4.05935596	7.1666E-07
1000	40	4.10569608	4.10569611	6.5256E-07
				Max. (%) 7.1041E-06

Fig. 4 visualizes the same deviations and confirms a smooth, single-hump residual with no oscillatory behaviour, evidence that the explicit expression preserves monotonicity and numerical conditioning. The dynamic range on the vertical axis is at the 10^{-6} % level, so the curve is effectively flat at publication scale; nevertheless, the plot captures the precise location of the worst-case point near $\xi \approx 50$.

Bottom line. Table 4 and Fig. 4 convincingly demonstrate that the explicit $\eta(\xi)$ relationship in Eq. (37) achieves quasi-exact performance across the full operating range, with a tiny and well-behaved residual. This level of accuracy, together with the documented worst-case location, provides strong assurance for deployment in routine engineering calculations.

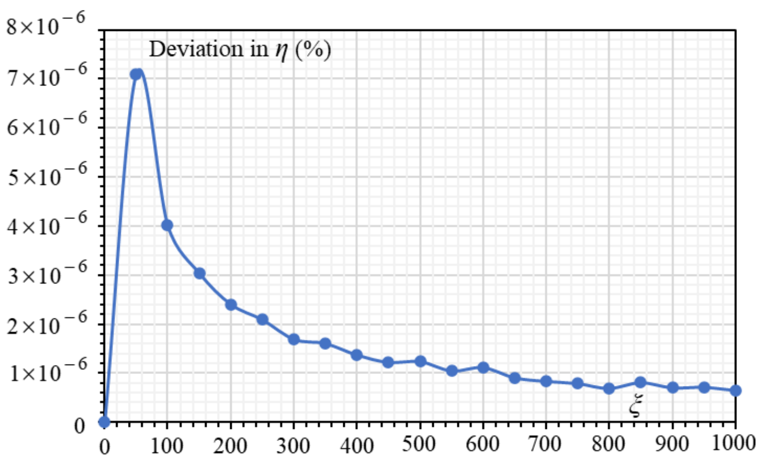

Figure 4: Distribution of the deviation (%) produced by the approximate Eq. (37) within the full range $\xi \in$ [0, 1000]

Asymptotic

It is interesting at this stage to pass to the limiting cases of Eq. (37). The first asymptote forms the case of a very wide trapezoidal channel base width, i.e., $b \to \infty$, corresponding to the following, according to Eq. (3b):

$$\xi \to 0$$

Also, in this case, the critical flow depth asymptotically tends to that of a rectangular shaped channel, according to Eq. (3b), corresponding to the following:

$$m \to 0$$

For that, if we substitute $\phi = 4\xi^{1/3}$ in Eq. (37) and expand in McLaurin series, around $\xi = 0$, one may obtain the following:

$$\eta = \xi^{1/3} - \frac{1}{3}\xi^{2/3} + \frac{55}{81}\xi^{4/3} - \frac{392}{243}\xi^{5/3} + \cdots \tag{38}$$

It is easy to show that that the expansion of Eq. (38) converges to the following limit:

$$\frac{h_c}{b} = \left(\frac{\alpha Q^2}{b^5 g \cos\theta} \right)^{1/3} \tag{39}$$

As it can be seen, Eq. (39) corresponds to the expression of the critical flow depth in a rectangular channel.

The other limiting case forming the second asymptote of the problem is when the following is reached:

$$b \to 0$$

or equivalently to what Eq. (3b) provides as follows:

$$\xi \to \infty$$

Expanding now Eq. (37) in an asymptotic series, one obtains:

$$\eta = -\frac{1}{2} + \left(2\xi\right)^{1/5} + \frac{3}{40}\left(\frac{2^4}{\xi}\right)^{1/5} - \frac{5183}{691200}\left(\frac{2^{2/3}}{\xi}\right)^{3/5} + \cdots \tag{40}$$

This case is related to the triangular cross-section channel for which the critical depth is explicitly given by the following:

$$h_c^5 = \frac{2\alpha Q^2}{m^2 g \cos\theta} \tag{41}$$

which forms the limit of the convergent series in Eq. (40). To show simply the convergence of the series (38) and (40), let us operate a change of variables such that we denote η^* and ξ^* as follows:

$$\eta^* = \frac{h_c}{b} \tag{42}$$

and

$$\xi^* = \frac{\alpha Q^2}{b^5 g \cos\theta} \tag{43}$$

Then, from the critical flow condition expressed by Eq. (4), the following can be written:

$$\xi^* = \frac{\left(m\eta^* + m\eta^{*2}\right)^3}{1 + 2m\eta^*} \tag{44}$$

From that, it is straightforward to show that the two limiting cases, i.e.:

$$\xi \to 0$$

and

$$\xi \to \infty$$

correspond respectively to what follows:

$$\eta_0^* = \xi^{*1/3} \tag{45}$$

$$\eta_\infty^* = \left(\frac{2\xi}{m}\right)^{1/5} \tag{46}$$

which correspond to the first term of the series in Eqs. (15) and (17). Operating in this way, the formal convergence analysis of the aforementioned series, in a classical way, is shifted to a simpler fact of checking only the correspondence of the first term of the series.

MAIN FINDINGS OF THE STUDY

Exact foundation and uniqueness

The critical-depth problem is recast as an exact mapping $\eta = z(\xi)$ [Eq. (5)], with the physical solution characterized as the unique positive root of a trinomial sextic [Eq. (5a)] or via exact inverse-function representations, i.e., residue integral and Lagrange–Bürmann/hypergeometric–Appell forms. These provide a machine-precision reference and explain why a simple radical form is unavailable.

Normalized one-unknown route (computational backbone)

A fifth-root scaling reduces the problem to a strictly monotone scalar equation in a single unknown [Eqs. (5i) – (5k)], from which a reduced form is obtained [Eqs. (5n) – (5o)]. The authors construct a closed-form rational seed $u_0(C)$, Eq. (5p) with coefficients in Eq. (5q), delivering a worst-case deviation < 0.002 % over the broad range $\xi \in [0.001, 1000]$; the worst case occurs at $\xi = 0.001$. A one-step Newton/Halley update [Eq. (5r)] then achieves near machine precision across the full range of ξ.

Single explicit (blended) formula for $z(\xi)$

For non-iterative, spreadsheet-ready use, a blended approximation merges rigorously matched small- and large-ξ branches with a smooth Hill-type switch [Eqs. (6) – (9)]. On the practical interval $\xi \in [0.001, 100]$ it achieves uniform, sub-6.5×10^{-5} deviations; on [100, 1000] it remains highly accurate, with a minimal deep-branch enrichment further flattening the tail.

Direct explicit $\eta(\xi)$ relationship

A well-conditioned change of variables and controlled asymptotic–Taylor construction yields a closed-form $\eta(\xi)$ [Eq. (37)] that is quasi-exact on $\xi \in [0, 1000]$, with a worst-case relative deviation $\approx 7.1\times10^{-6}$ % at $\xi = 50$.

Traceable error propagation

An analytic mapping quantifies how errors in z transfer to η and design variables [Eq. (17)], ensuring that reported numerical accuracy is meaningful hydraulically.

Implementation guidance and verification

Beyond formulas, the manuscript supplies practical guidance: how to pick robust starting values, how to bracket safely, and how to evaluate the exact integral representation when desired. The accompanying Tables and Figures certify monotonicity, identify the worst-case location and magnitude, and demonstrate the absence of spurious oscillations across the range.

CONCLUSION

This study delivers a complete, verification-driven solution to the critical-depth problem in trapezoidal channels by connecting exact analysis with deployable formulas that are both fast and exceptionally accurate. At the theoretical core is the exact mapping $\eta = z(\xi)$ [Eq. (5)], which establishes existence, uniqueness, and a machine-precision benchmark through its sextic characterization [Eq. (5a)] and analytic inversions. This "ground truth" explains why a simple radical form is unavailable and anchors everything that follows.

Building on that foundation, the paper introduces a normalized one-unknown route that collapses the computation to a strictly monotone scalar equation [Eqs. (5i) – (5k)]. From this normalized form, the authors construct a closed-form rational seed $u_0(C)$ [Eq. (5p), coefficients in Eq. (5q)] with a worst-case deviation below 0.002% over $\xi \in [0.001, 1000]$; a single Newton/Halley update [Eq. (5r)] then attains near machine precision across the entire range. This yields a quasi-exact "one-step" workflow that requires neither charts nor special functions, and is robust in both the shallow- and deep-ξ limits.

For non-iterative use, i.e., hand calculations, spreadsheets, embedded design tools, a single explicit blended approximation for $z(\xi)$ merges rigorously matched small- and large-ξ branches with a smooth Hill-type switch [Eqs. (6) – (9)]. On $\xi \in [0.001, 100]$ it maintains uniform, sub-6.5×10^{-5} % deviations; on [100, 1000], it remains highly accurate, with a minimal deep-branch enrichment available to flatten the far-tail if needed. The residuals are smooth and single-humped, confirming good conditioning and the absence of spurious oscillations.

The manuscript also provides a direct explicit relationship $\eta(\xi)$ [Eq. (37)], obtained via a well-conditioned change of variables and controlled asymptotic–Taylor construction. This closed-form expression is quasi-exact over $\xi \in [0, 1000]$, with a worst-case relative deviation of about 7.1×10^{-6} %, at $\xi = 50$.

Together with a transparent error-propagation mapping from z to η and design variables [Eq. (17)], the paper ensures that numerical accuracy is meaningful hydraulically and traceable in downstream calculations.

Declaration of competing interest

The authors declare that they have no known competing financial interests or personal relationships that could have appeared to influence the work reported in this paper.

REFERENCES

ACHOUR B., AMARA L. (2020a). New theoretical considerations on the critical flow in a circular conduit (Part 1), Larhyss Journal, No 43, pp. 103-118.

ACHOUR B., AMARA L. (2020b). Critical flow in a rectangular-shaped channel, Larhyss Journal, No 44, pp. 57-72.

ACHOUR B., AMARA L. (2020c). Critical Flow in a Triangular-Shaped Channel, Larhyss Journal, No 44, pp. 43-55.

ACHOUR B., AMARA L. (2020d). New theoretical considerations on the critical flow in a circular conduit (Part 2), Larhyss Journal, No 44, pp. 31-41.

ACHOUR B., BEDJAOUI A. (2006). Discussion to " Exact solution for normal depth problem, by Swamme P.K. and Rathie P.N".,Journal of Hydraulic Research, Vol. 44, Issue 5, pp.715-717.

ACHOUR B., KHATTAOUI M. (2008). Computation of Normal and Critical Depths in Parabolic Cross Sections, Open Civil Engineering Journal, No 2, pp 9-14.

ACHOUR B., NEBBAR M. (2015). New Approach for the Calculation of Critical Depth in a U-Shaped Channel, Journal of Scientific Research and Reports, Vol.8, Issue 6, pp. 1-6.

AMARA L., ACHOUR B. (2023). Delta-Perturbation Expansion for Critical Flow Depth Problem in Trapezoidal Channels, Flow Measurement and Instrumentation, Vol. 91, Paper ID 102362.

BENDER C.M., MILTON K.A., PINSKY S.S., SIMMONS Jr. L.M. (1989). A new perturbative approach to nonlinear problems, Journal of Mathematical Physics, Vol. 30, Issue 7, pp. 1447-1455.

CHENG T., WANG J., SUI J. (2018). Calculation of critical flow depth using method of algebraic inequality, Journal of Hydrology and Hydromechanics, Vol. 66, Issue 3, pp. 316–322.

CHOW V.T. (1959). Open Channel Hydraulics, Book, McGray-Hill, New York, USA.

ELHAKEEM M. (2017). Explicit solution for flow depth in open channels of trapezoidal cross-sectional area: classic problem of interest, Journal of Irrigation and Drainage Engineering, Vol. 143, Issue 7, Paper ID 04017011.

FRENCH R.H. (1987). Open channel hydraulics, Book, McGraw-Hil, New York, NY, USA.

HACHEMI-RACHEDI L., LAKEHAL M., ACHOUR B. (2021). Modern vision for critical flow in an egg-shaped section, Water Science and Technology, Vol. 84, Issue 4, pp.840-850.

HAGER W.H. (1985). Critical flow condition in open channel hydraulics, Acta Mechanica, No 54, pp.157-179.

HAGER W.H. (2010). Wastewater hydraulics: Theory and practice, 2nd Edition, Springer - Berlin Heidelberg.

HENDERSON M. F. (1966). Open channel flow, Book, MacMillan, New York, NY, USA.

KREYSZIG E. (1979). Advanced Engineering Mathematics, Book, 4th Edition., Wiley and Sons, New York, NY, USA.

LAKEHAL M., ACHOUR B. (2017). New approach for the normal depth computation in a trapezoidal open channel using the rough model method, Larhyss Journal, No 32, pp. 269-284.

LI F., WEN H., LIN X. (2012). A new formula for critical depth of the U-shaped channels, Applied Mechanics and Materials, Vols. 212–213, pp. 1136-1140.

LIU J.L., WANG Z.Z., LENG C.J., ZHAO Y.F. (2012). Explicit equations for critical depth in open channels with complex compound cross sections, Flow Measurement and Instrumentation, Vol. 24, pp. 13-18.

NEBBAR M.L., ACHOUR B. (2018). Design of rectangular channel at critical flow, Larhyss Journal, No 34, pp. 7-20.

SEHTAL S., ACHOUR B. (2023). Normal depth computation in a vaulted rectangular channel using the rough model method (RMM), Larhyss Journal, No 54, pp. 193-216.

SEHTAL S., ACHOUR B. (2024). A New Vision of the Critical flow in a Parabolic Channel (Part 1), Larhyss Journal, No 57, pp. 159-173.

SHANG H., XU, S., ZHANG K., ZHAO L. (2019). Explicit solution for critical depth in closed conduits flowing partly full, Water, Vol. 11, No 10.

SWAMEE P.K. (1993). Critical Depth Equations for Irrigation Canals, Journal of Irrigation and Drainage Engineering, Vol. 119, No 2, pp. 400-409.

SWAMEE P.K. (1994). Normal-depth equations for irrigation canals, Journal of Irrigation and Drainage Engineering, Vol. 120, Issue 5, pp. 942-948.

SWAMEE P.K., RATHIE P.N. (2005). Exact equations for critical depth in a trapezoidal canal, Journal of Irrigation and Drainage Engineering, Vol. 131, Issue 5, pp. 474-476.

VARANDILI S.A., ARVANAGHI H., GHORBANI M.A., YASEEN Z.M. (2019). A novel and exact analytical model for determination of critical depth in trapezoidal open channels, Flow Measurement and Instrumentation, Vol. 68, Paper ID 101575.

VATANKHAH A.R. (2013). Explicit solutions for critical and normal depths in trapezoidal and parabolic open channels, Ain Shams Engineering Journal, Vol. 4, pp. 17-23.

VATANKHAH A.R., EASA S.M. (2011). Explicit solutions for critical and normal depths in channels with different shapes. Flow Measurement and Instrumentation, Vol. 22, Issue 1, pp. 43-49.

WANG Z. (1998). Formula for calculating critical depth of trapezoidal open channel, Journal of Hydraulic Engineering, Vol. 124, Vol. 1, pp. 90-91.

WONG T.S.W., ZHOU M.C. (2004). Determination of critical and normal depths using Excel. Proceedings of the 2004 World Water and Environmental Resources Congress: Critical Transitions in Water and Environmental Resources Management, pp. 1380-1387.